Welfare of Japan, The Program for the Promotion of Fundamental Studies in Health Science of the National Institute of Biomedical Innovation. The authors declare no conflict of interest.

Supporting information

Additional supporting information may be found in the online version of this article:

Figure S1. Administration of NMDA-R antagonist does not affect the total number of Dcx+ immature neurons.

Figure S2. Exogenous expression of GFP-DISC1 does not affect the expression of NDEL1.

Figure S3. Administration of memantine reduces *DISC1* mRNA expression in the embryonic neocortex.

Figure S4. Administration of NMDA-R antagonist does not affect the CaMKII expression and its phosphorylation.

As a service to our authors and readers, this journal provides supporting information supplied by the authors. Such materials are peer-reviewed and may be re-organized for online delivery, but are not copy-edited or typeset. Technical support issues arising from supporting information (other than missing files) should be addressed to the authors.

References

Adachi Y. U., Watanabe K., Satoh T. and Vizi E. S. (2001) Halothane potentiates the effect of methamphetamine and nomifensine on extracellular dopamine levels in rat striatum: a microdialysis study. *Br. J. Anaesth.* **86**, 837–845.

Austin C. P., Ky B., Ma L., Morris J. A. and Shughrue P. J. (2004) Expression of Disrupted-In-Schizophrenia-1, a schizophrenia-associated gene, is prominent in the mouse hippocampus throughout brain development. *Neuroscience* **124**, 3–10.

Behar T. N., Scott C. A., Greene C. L., Wen X., Smith S. V., Maric D., Liu Q. Y., Colton C. A. and Barker J. L. (1999) Glutamate acting at NMDA receptors stimulates embryonic cortical neuronal migration. *J. Neurosci.* **19**, 4449–4461.

Brandon N. J., Handford E. J., Schurov I. *et al.* (2004) Disrupted in Schizophrenia 1 and Nudel form a neurodevelopmentally regulated protein complex: implications for schizophrenia and other major neurological disorders. *Mol. Cell. Neurosci.* **25**, 42–55.

Cameron H. A., McEwen B. S. and Gould E. (1995) Regulation of adult neurogenesis by excitatory input and NMDA receptor activation in the dentate gyrus. *J. Neurosci.* **15**, 4687–4692.

Chubb J. E., Bradshaw N. J., Soares D. C., Porteous D. J. and Millar J. K. (2008) The DISC locus in psychiatric illness. *Mol. Psychiatry* **13**, 36–64.

DeCarolis N. A. and Eisch A. J. (2010) Hippocampal neurogenesis as a target for the treatment of mental illness: a critical evaluation. *Neuropharmacology* **58**, 884–893.

Denter D. G., Heck N., Riedemann T., White R., Kilb W. and Luhmann H. J. (2010) GABAC receptors are functionally expressed in the intermediate zone and regulate radial migration in the embryonic mouse neocortex. *Neuroscience* **167**, 124–134.

Dhavan R., Greer P. L., Morabito M. A., Orlando L. R. and Tsai L. H. (2002) The cyclin-dependent kinase 5 activators p35 and p39 interact with the alpha-subunit of Ca^{2+}/calmodulin-dependent protein kinase II and alpha-actinin-1 in a calcium-dependent manner. *J. Neurosci.* **22**, 7879–7891.

Duan X., Chang J. H., Ge S. *et al.* (2007) Disrupted-In-Schizophrenia 1 regulates integration of newly generated neurons in the adult brain. *Cell* **130**, 1146–1158.

Enomoto A., Asai N., Namba T. *et al.* (2009) Roles of disrupted-in-schizophrenia 1-interacting protein girdin in postnatal development of the dentate gyrus. *Neuron* **63**, 774–787.

Fukumura M., Cappon G. D., Pu C., Broening H. W. and Vorhees C. V. (1998) A single dose model of methamphetamine-induced neurotoxicity in rats: effects on neostriatal monoamines and glial fibrillary acidic protein. *Brain Res.* **806**, 1–7.

Hattori M., Adachi H., Tsujimoto M., Arai H. and Inoue K. (1994) Miller-Dieker lissencephaly gene encodes a subunit of brain platelet-activating factor acetylhydrolase [corrected]. *Nature* **370**, 216–218.

Heng J. I., Moonen G. and Nguyen L. (2007) Neurotransmitters regulate cell migration in the telencephalon. *Eur. J. Neurosci.* **26**, 537–546.

Hirasawa T., Wada H., Kohsaka S. and Uchino S. (2003) Inhibition of NMDA receptors induces delayed neuronal maturation and sustained proliferation of progenitor cells during neocortical development. *J. Neurosci. Res.* **74**, 676–687.

Hirotsune S., Fleck M. W., Gambello M. J., Bix G. J., Chen A., Clark G. D., Ledbetter D. H., McBain C. J. and Wynshaw-Boris A. (1998) Graded reduction of Pafah1b1 (Lis1) activity results in neuronal migration defects and early embryonic lethality. *Nat. Genet.* **19**, 333–339.

Hood W. F., Compton R. P. and Monahan J. B. (1989) D-cycloserine: a ligand for the N-methyl-D-aspartate coupled glycine receptor has partial agonist characteristics. *Neurosci. Lett.* **98**, 91–95.

Imperato A., Scrocco M. G., Bacchi S. and Angelucci L. (1990) NMDA receptors and in vivo dopamine release in the nucleus accumbens and caudatus. *Eur. J. Pharmacol.* **187**, 555–556.

Jin K., Xie L., Mao X. O. and Greenberg D. A. (2006) Alzheimer's disease drugs promote neurogenesis. *Brain Res.* **1085**, 183–188.

Kamiya A., Kubo K., Tomoda T. *et al.* (2005) A schizophrenia-associated mutation of DISC1 perturbs cerebral cortex development. *Nat. Cell Biol.* **7**, 1167–1178.

Kim J. Y., Duan X., Liu C. Y., Jang M. H., Guo J. U., Pow-anpongkul N., Kang E., Song H. and Ming G. L. (2009) DISC1 regulates new neuron development in the adult brain via modulation of AKT-mTOR signaling through KIAA1212. *Neuron* **63**, 761–773.

Kitayama T., Yoneyama M., Tamaki K. and Yoneda Y. (2004) Regulation of neuronal differentiation by N-methyl-D-aspartate receptors expressed in neural progenitor cells isolated from adult mouse hippocampus. *J. Neurosci. Res.* **76**, 599–612.

Kodomari I., Maruoka T., Yamauchi R., Wada E. and Wada K. (2009) Ghrelin alters postnatal endocrine secretion and behavior in mouse offspring. *Neurochem. Int.* **54**, 222–228.

Kuhn H. G., Dickinson-Anson H. and Gage F. H. (1996) Neurogenesis in the dentate gyrus of the adult rat: age-related decrease of neuronal progenitor proliferation. *J. Neurosci.* **16**, 2027–2033.

Kvajo M., McKellar H., Arguello P. A., Drew L. J., Moore H., MacDermott A. B., Karayiorgou M. and Gogos J. A. (2008) A mutation in mouse Disc1 that models a schizophrenia risk allele leads to specific alterations in neuronal architecture and cognition. *Proc. Natl Acad. Sci. USA* **105**, 7076–7081.

Maekawa M., Namba T., Suzuki E., Yuasa S., Kohsaka S. and Uchino S. (2009) NMDA receptor antagonist memantine promotes cell proliferation and production of mature granule neurons in the adult hippocampus. *Neurosci. Res.* **63**, 259–266.

Manent J. B. and Represa A. (2007) Neurotransmitters and brain maturation: early paracrine actions of GABA and glutamate modulate neuronal migration. *Neuroscientist* **13**, 268–279.

Mares P. and Velisek L. (1992) N-methyl-D-aspartate (NMDA)-induced seizures in developing rats. *Brain Res. Dev. Brain Res.* **65**, 185–189.

Millar J. K., Wilson-Annan J. C., Anderson S. *et al.* (2000) Disruption of two novel genes by a translocation co-segregating with schizophrenia. *Hum. Mol. Genet.* **9**, 1415–1423.

Millar J. K., Pickard B. S., Mackie S. *et al.* (2005) DISC1 and PDE4B are interacting genetic factors in schizophrenia that regulate cAMP signaling. *Science* **310**, 1187–1191.

Ming G. L. and Song H. (2005) Adult neurogenesis in the mammalian central nervous system. *Annu. Rev. Neurosci.* **28**, 223–250.

Nacher J. and McEwen B. S. (2006) The role of N-methyl-D-asparate receptors in neurogenesis. *Hippocampus* **16**, 267–270.

Nacher J., Rosell D. R., Alonso-Llosa G. and McEwen B. S. (2001) NMDA receptor antagonist treatment induces a long-lasting increase in the number of proliferating cells, PSA-NCAM-immunoreactive granule neurons and radial glia in the adult rat dentate gyrus. *Eur. J. Neurosci.* **13**, 512–520.

Namba T., Mochizuki H., Onodera M., Mizuno Y., Namiki H. and Seki T. (2005) The fate of neural progenitor cells expressing astrocytic and radial glial markers in the postnatal rat dentate gyrus. *Eur. J. Neurosci.* **22**, 1928–1941.

Namba T., Maekawa M., Yuasa S., Kohsaka S. and Uchino S. (2009) The Alzheimer's disease drug memantine increases the number of radial glia-like progenitor cells in adult hippocampus. *Glia* **57**, 1082–1090.

Namba T., Yabe T., Gonda Y., Ichikawa N., Sanagi T., Arikawa-Hirasawa E., Mochizuki H., Kohsaka S. and Uchino S. (2010) Pigment epithelium-derived factor up-regulation induced by memantine, an N-methyl-D-aspartate receptor antagonist, is involved in increased proliferation of hippocampal progenitor cells. *Neuroscience* **167**, 372–383.

Niethammer M., Smith D. S., Ayala R., Peng J., Ko J., Lee M. S., Morabito M. and Tsai L. H. (2000) NUDEL is a novel Cdk5 substrate that associates with LIS1 and cytoplasmic dynein. *Neuron* **28**, 697–711.

O'Donnell J., Stemmelin J., Nitta A., Brouillette J. and Quirion R. (2003) Gene expression profiling following chronic NMDA receptor blockade-induced learning deficits in rats. *Synapse* **50**, 171–180.

Ozeki Y., Tomoda T., Kleiderlein J. *et al.* (2003) Disrupted-in-Schizophrenia-1 (DISC-1): mutant truncation prevents binding to NudE-like (NUDEL) and inhibits neurite outgrowth. *Proc. Natl Acad. Sci. USA* **100**, 289–294.

Paulson L., Martin P., Persson A., Nilsson C. L., Ljung E., Westman-Brinkmalm A., Eriksson P. S., Blennow K. and Davidsson P. (2003) Comparative genome- and proteome analysis of cerebral cortex from MK-801-treated rats. *J. Neurosci. Res.* **71**, 526–533.

Reiner O., Carrozzo R., Shen Y., Wehnert M., Faustinella F., Dobyns W. B., Caskey C. T. and Ledbetter D. H. (1993) Isolation of a Miller-Dieker lissencephaly gene containing G protein beta-subunit-like repeats. *Nature* **364**, 717–721.

Sasaki S., Shionoya A., Ishida M., Gambello M. J., Yingling J., Wynshaw-Boris A. and Hirotsune S. (2000) A LIS1/NUDEL/cytoplasmic dynein heavy chain complex in the developing and adult nervous system. *Neuron* **28**, 681–696.

Seki T. and Arai Y. (1993) Highly polysialylated neural cell adhesion molecule (NCAM-H) is expressed by newly generated granule cells in the dentate gyrus of the adult rat. *J. Neurosci.* **13**, 2351–2358.

Seki T. and Arai Y. (1995) Age-related production of new granule cells in the adult dentate gyrus. *Neuroreport* **6**, 2479–2482.

Seki T., Namba T., Mochizuki H. and Onodera M. (2007) Clustering, migration, and neurite formation of neural precursor cells in the adult rat hippocampus. *J. Comp. Neurol.* **502**, 275–290.

Shinoda T., Taya S., Tsuboi D., Hikita T., Matsuzawa R., Kuroda S., Iwamatsu A. and Kaibuchi K. (2007) DISC1 regulates neurotrophin-induced axon elongation via interaction with Grb2. *J. Neurosci.* **27**, 4–14.

Shoblock J. R., Sullivan E. B., Maisonneuve I. M. and Glick S. D. (2003) Neurochemical and behavioral differences between d-methamphetamine and d-amphetamine in rats. *Psychopharmacology (Berl)* **165**, 359–369.

Spanagel R., Eilbacher B. and Wilke R. (1994) Memantine-induced dopamine release in the prefrontal cortex and striatum of the rat–a pharmacokinetic microdialysis study. *Eur. J. Pharmacol.* **262**, 21–26.

Tashiro A., Sandler V. M., Toni N., Zhao C. and Gage F. H. (2006) NMDA-receptor-mediated, cell-specific integration of new neurons in adult dentate gyrus. *Nature* **442**, 929–933.

Taya S., Shinoda T., Tsuboi D. *et al.* (2007) DISC1 regulates the transport of the NUDEL/LIS1/14-3-3epsilon complex through kinesin-1. *J. Neurosci.* **27**, 15–26.

Tozuka Y., Fukuda S., Namba T., Seki T. and Hisatsune T. (2005) GABAergic excitation promotes neuronal differentiation in adult hippocampal progenitor cells. *Neuron* **47**, 803–815.

Uchino S., Hirasawa T., Tabata H., Gonda Y., Waga C., Ondo Y., Nakajima K. and Kohsaka S. (2010) Inhibition of N-methyl-d-aspartate receptor activity resulted in aberrant neuronal migration caused by delayed morphological development in the mouse neocortex. *Neuroscience* **169**, 609–618.

Wang Y. and Baraban S. C. (2007) Granule cell dispersion and aberrant neurogenesis in the adult hippocampus of an LIS1 mutant mouse. *Dev. Neurosci.* **29**, 91–98.

Wojtowicz J. M., Askew M. L. and Winocur G. (2008) The effects of running and of inhibiting adult neurogenesis on learning and memory in rats. *Eur. J. Neurosci.* **27**, 1494–1502.

Yamasaki N., Maekawa M., Kobayashi K. *et al.* (2008) Alpha-CaMKII deficiency causes immature dentate gyrus, a novel candidate endophenotype of psychiatric disorders. *Mol. Brain* **1**, 6.

Yang F. Y., Lee Y. S., Cherng C. G., Cheng L. Y., Chang W. T., Chuang J. Y., Kao G. S. and Yu L. (2010) D-cycloserine, sarcosine and D-serine diminish the expression of cocaine-induced conditioned place preference. *J. Psychopharmacol.* Published Online doi: 10.1177/0269881110388333.

Novel variants of the *SHANK3* gene in Japanese autistic patients with severe delayed speech development

Chikako Waga[a], Nobuhiko Okamoto[c], Yumiko Ondo[a], Reiko Fukumura-Kato[a], Yu-ichi Goto[b], Shinichi Kohsaka[a] and Shigeo Uchino[a]

The 22q13.3 deletion syndrome is characterized by a significant delay in language development, mental retardation, hypotonia, and autistic features. Cumulative evidence has shown that haploinsufficiency of the *SHANK3* gene is a major cause of the neurological symptoms of the 22q13.3 deletion syndrome. Shank3, a multidomain protein containing the SH3 and PDZ domains, is thought to play an important role in the formation and function of synapses in the developing brain. In this study, we analyzed the *SHANK3* gene in 128 autistic patients with manifestations similar to those seen in the 22q13.3 deletion syndrome. The results showed a 6-amino acid deletion upstream of the SH3 domain, a missense variant (arginine to histidine at amino acid position 656) in the PDZ domain, and the insertion or deletion of a repeated 10-bp GC sequence located 9-bp downstream from the 3′ end of exon 11. None of these variants was found in 228 controls. *Psychiatr Genet* 21:208–211 © 2011 Wolters Kluwer Health | Lippincott Williams & Wilkins.

Psychiatric Genetics 2011, 21:208–211

Keywords: 22q13.3 deletion syndrome, autism spectrum disorder, CpG island, mental retardation, Shank3, synapse

Departments of [a]Neurochemistry, [b]Mental Retardation and Birth Defect Research, National Institute of Neuroscience, Tokyo and [c]Department of Medical Genetics, Osaka Medical Center and Research Institute for Maternal and Child Health, Osaka, Japan

Correspondence to Shinichi Kohsaka, MD, PhD, Department of Neurochemistry, National Institute of Neuroscience, 4-1-1 Ogawahigashi, Kodaira, Tokyo 187-8502, Japan
Tel: +81 42 346 1711; fax: +81 42 346 1741;
e-mail: kohsaka@ncnp.go.jp

Received 17 March 2010 **Revised** 4 October 2010
Accepted 21 October 2010

Introduction

A terminal 22q13.3 deletion is one of the more common submicroscopic sub telomere deletions found in patients with mental retardation, and the 22q13.3 deletion syndrome is characterized by severe expressive language and speech delay, hypotonia, global developmental delay, normal-to-advanced growth, and minor dysmorphisms, including a prominent forehead and autistic features are also often exhibited (Phelan *et al.*, 2001; Manning *et al.*, 2004). Recent genetic analyses carried out in several patients with the 22q13.3 deletion syndrome have identified *SHANK3* (also known as *PROSAP2*) as a candidate gene for the etiology of the neuropathological manifestations observed in this syndrome (Bonaglia *et al.*, 2001; Wilson *et al.*, 2003; Bonaglia *et al.*, 2006).

The *SHANK3* gene consists of 22 exons and encodes a multidomain protein that contains an SH3 domain, a PDZ domain, ankyrin repeats, a homer-binding region, and a cortactin-binding region (Naisbitt *et al.*, 1999). Shank3 is mainly expressed in neurons, especially in their synapses, and its tissue-specific expression is regulated by DNA methylation within CpG islands (Beri *et al.*, 2007). Shank3 acts as a scaffolding protein in its interactions with various synaptic molecules, including postsynaptic density-95 and α-amino-3-hydroxy-5-methyl-4-isoxazole-propionic acid receptors (Lim *et al.*, 1999; Naisbitt *et al.*, 1999; Sheng and Kim, 2000; Böckers *et al.*, 2002; Uchino *et al.*, 2006). Several mutations within the *SHANK3* gene have recently been found in patients with autism spectrum disorders (ASDs) (Durand *et al.*, 2007; Moessner *et al.*, 2007; Gauthier *et al.*, 2008).

To further assess the contribution of SHANK3 to the pathogenesis of ASDs, we analyzed the *SHANK3* gene in 128 autistic patients with mental disorders who exhibited severe delayed speech and language development that resembled the characteristics of the 22q13.3 deletion syndrome but in the absence of a 22q terminal deletion, and we identified novel variants in the *SHANK3* gene.

Methods

Patients

We examined patients by physical examination, electroencephalography (EEG), computed tomography scan of the brain, MRI, and diagnosed them with an ASD according to the Diagnostic and Statistical Manual of Mental Disorders-fourth edition criteria. Every patient was also examined clinically for dysmorphism. Some patients were suspected of having a Fragile-X phenotype, but the results of the clinical examination were negative in every patient except one, and that patient was excluded from this study. The Kyoto style Developmental Quotient (DQ) test (Japanese standard test for DQ) or Wechsler Intelligence Scale for Children-third edition (revised) was used as a DQ test in most patients. We initially selected 134 patients who exhibited manifestations similar to those of the 22q13.3 deletion syndrome

0955-8829 © 2011 Wolters Kluwer Health | Lippincott Williams & Wilkins

DOI: 10.1097/YPG.0b013e328341e069

that is characterized by severe expressive language delay, mental retardation, hypotonia, minor dysmorphisms (dolichocephaly, epicanthic folds, saddle nose with bulbous tip, abnormal ears, ptosis), dysplastic toe nails, increased tolerance to pain, relatively large hands and normal to advanced growth (Phelan *et al.*, 2001), and chromosome testing, including by fluorescent in-situ hybridization analysis with a *SHANK3*-specific probe, which showed that six patients had a deletion of the entire *SHANK3* gene (22q13.3 deletion syndrome). In this study we carried out *SHANK3* gene analysis by a DNA sequencing technique on the 128 patients who did not have any major chromosome abnormalities, including a *SHANK3* gene deletion. The 228 controls were selected from the cognitively intact patients with Alzheimer's disease (Tanaka *et al.*, 2010). Informed consent to use peripheral blood samples from the patients for genetic research was obtained. This study was approved by the ethics committee of each of our institutes.

Sequencing of genomic DNA

Genomic DNA was extracted from peripheral blood leukocytes and the genomic sequence of the *SHANK3* gene was analyzed by using an ABI3100-*avant* genetic analyzer (Applied Biosystems, Foster City, California, USA) according to the standard protocols. Some of the primers for PCR were obtained from Durand *et al.* (2007) and three additional primers were used, that is, 5′-GCAGCGCGGCCGACGGGGCT-3′, a forward primer for exon1-2 (accession no. NT_011526); 5′-ACCCGCACGGCAGGAACCTT-3′, a reverse primer for exon11 (accession no. DQ_173561); and 5′-GATGG GAAGAGGAATGTGGGCCT-3′, a reverse primer for exon16 (accession no. NT_011526). Detailed information on the PCR conditions will be provided on request. We initially performed direct sequencing to screen for variants. To determine the DNA sequence of heterozygous variants, we subcloned the genomic PCR product into the pUC119 vector and confirmed the sequences.

Reverse transcription PCR

Leukocytes were isolated from fresh peripheral blood using a red blood cell lysis solution (Promega, Madison, Wisconsin, USA), and total RNA was extracted from leukocytes using a SV total RNA isolation system (Promega). The cDNA was synthesized using an advantage RT for PCR kit (Clontech, Palo Alto, California, USA). PCR was performed using PrimeSTAR GXL DNA polymerase (TAKARA, Shiga, Japan) and a thermal cycler (GeneAmp PCR System 9700; Applied Biosystems). The thermocycle conditions were: 60 s at 98°C, 30 s at 50°C, and 60 s at 68°C for 40 cycles. The primers were: a forward primer SHANK3RT3F, 5′-CAGGAGAGCA ACATCAGTGG-3′, and a reverse primer SHANK3RT8R, 5′-GCTGTAAAGTTTCCGCTTCG-3′.

Results and discussion

A novel heterozygous six-amino acid deletion (GPGPAP at 441-446, Fig. 1a) upstream of the SH3 domain was identified in a 3-year-old boy who exhibited an ASD, severe mental retardation, and delayed psychomotor development. The G-banded karyotype (46,XY), EEG, and MRI examinations showed no significant abnormal findings. The variant was inherited from the patient's mother, whose speech development was also delayed, but she had no problems with communication or social interaction. We confirmed the deletion by a reverse transcription PCR analysis of the peripheral blood leukocytes from the patient and his parent (Fig. 1b). Approximately 100-bp extra band was detected in the patient, but because it was very faint and there was poor reproducibility, we were unable to determine whether it was part of a *SHANK3* transcript. We also identified a novel heterozygous missense variant (R656H, Fig. 1c) within the PDZ domain in a 5-year-old boy with an ASD and mild mental retardation. At 4 years of age, his DQ was 67, and he could speak simple sentences. The G-banded karyotype (46,XY), EEG, and MRI examinations yielded normal findings. This variant was inherited from the patient's father, who is normal. We confirmed the missense R656H by a reverse transcription PCR analysis of the peripheral blood leukocytes from both the patient and his father. As the SH3 domain and PDZ domain are important to interaction with other synaptic molecules, such as postsynaptic density-95 and α-amino-3-hydroxy-5-methyl-4-isoxazolepropionic acid receptors (Lim *et al.*, 1999; Naisbitt *et al.*, 1999; Sheng and Kim, 2000; Böckers *et al.*, 2002; Uchino *et al.*, 2006), further study, including a biochemical analysis, is now in progress to elucidate the function of the Shank3 variants.

We identified a heterozygous insertion of a repeated 10-bp GC sequence in intron 11 (Fig. 1d) in three patients. Two of the three patients, patient 1, a 5-year-old girl and patient 2, a 4-year-old boy, are siblings born of healthy parents, and the other patient, patient 3, an 8-year-old girl, is the second child of healthy parents and has a healthy brother and sister. As the parents of patient 3 do not have the insertion, this variant is probably *de novo*. All three patients have a prominent forehead, and their head circumference is as follows: patient 1, 52.5 cm [+ 1.8 standard deviation (SD)]; patient 2, 52.5 cm (+ 2.0 SD); patient 3, 57.5 cm (+ 3.0 SD). Patient 1 and patient 3 are able to speak two-word phrases, but patient 2 cannot speak meaningful words, although he often spontaneously utters a few words. The G-banded karyotypes, EEG, and computed tomography examinations of the brain of all three patients were normal. We identified a heterozygous deletion of a repeated 10-bp GC sequence in the same region (Fig. 1d) in another patient, a 14-year-old boy, who is the third child of healthy parents and has two healthy sisters. At 11 years of age, his DQ was 18, and he did not speak any meaningful words, indicating that he had an

Fig. 1

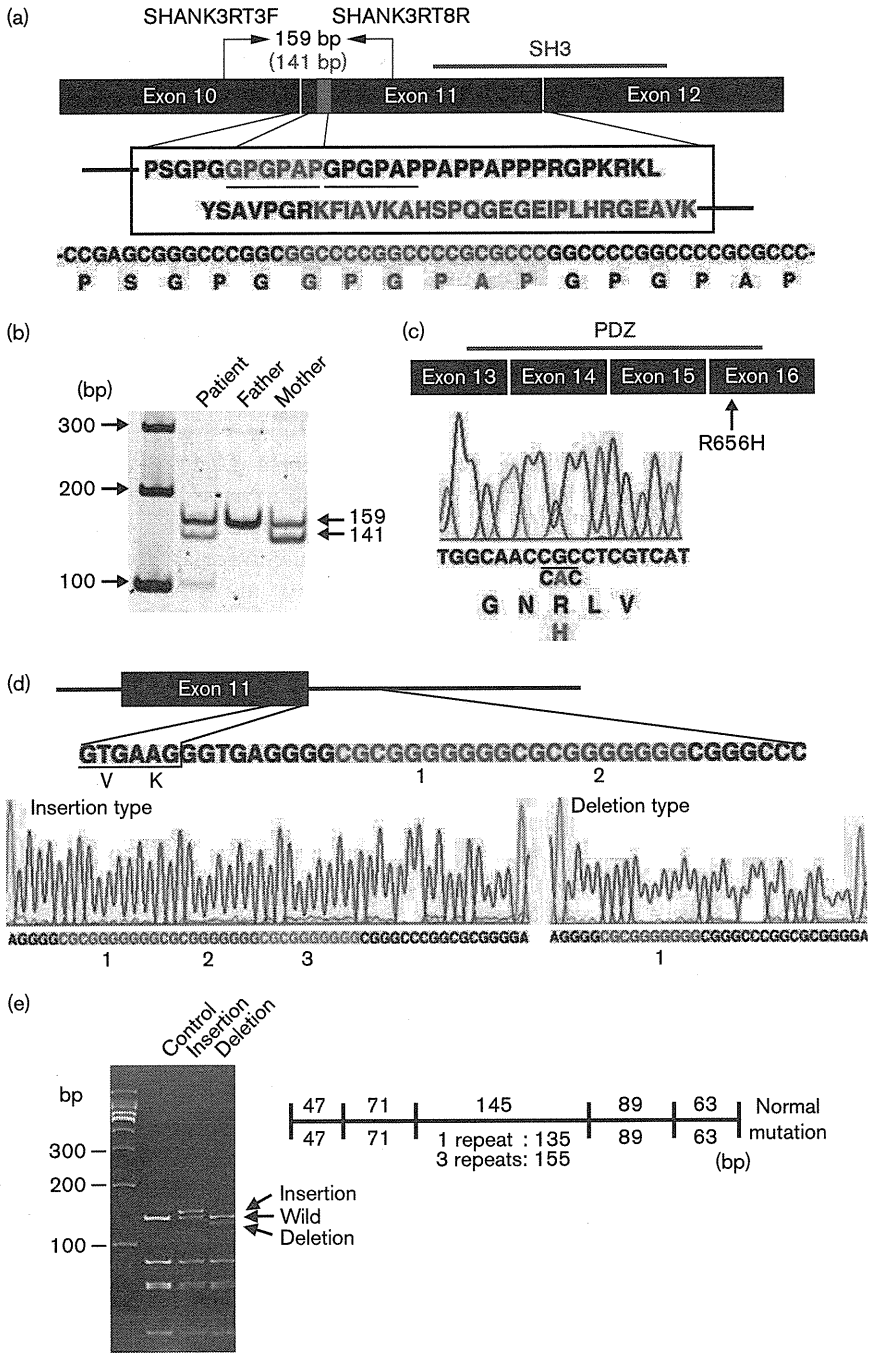

Novel variants of the *SHANK3* gene found in patients with autism spectrum disorders. (a) Schematic representation of the SH3 domain. The normal amino acid and cDNA sequencing profiles in exon 11 are shown. The red characters represent the deleted six amino acids (18-bp nucleotides) found in the patient. (b) Polyacrylamide gel electrophoresis of the reverse transcription PCR products visualized by staining with CYBR green. The primers used (SHANK3RT3F and SHANK3RT8R) are shown in the panel a. (c) Schematic representation and DNA sequence chromatograms of the PZD domain and missense variants (R656H). (d) Schematic representation and sequencing profile of normal genomic DNA (top). Colored characters represent the 10-bp GC sequence. DNA sequence chromatograms of the insertion-type variant (three repeats of the 10-bp GC sequence; left) and deletion-type variant (single 10-bp GC sequence; right). (e) polyacrylamide gel electrophoresis of genomic PCR products digested with *Apa*I and visualized by staining with ethidium bromide (left) and restriction enzyme map with *Apa*I in normal and mutated genomic PCR products (right).

ASD and severe mental retardation. In contrast to the patients with the insertion-type variant, his forehead was small, and his head circumferences was only 49.0 cm (−2.0 SD). He had a clinical history of mixed receptive–expressive language disorder, fine motor impairment, repetitive and compulsive tendencies, and poor social

Table 1 The *SHANK3* variants identified in patients with autism spectrum disorders

Region	Nucleotide change	Amino acid change	ASD sample				Control sample				Reference
			wt/wt	wt/mu	mu/mu	Total no. of sample	wt/wt	wt/mu	mu/mu	Total no. of sample	
Exon 5	c.483C/T		116	5	0	121	215	12	0	227	rs79762996
Exon 6	c.734T/C	p.245 Ile/Thr	76	42	4	122	151	66	10	227	rs9616915
Exon 6	c.750C/T		121	1	0	122	225	2	0	227	No
Exon 11	c.1320-1338 del	p.440-446 del. GPGPAP	127	1	0	128	228	0	0	228	No
Intron 11	c.1497+9 10bp/ins		125	3	0	128	228	0	0	228	No
Intron 11	c.1497+9 10bp/del		127	1	0	128	228	0	0	228	No
Exon 12	c.1563 G/A		123	1	0	124	216	0	0	216	No
Exon 16	c.1967 G/A	p.656 Arg/His	122	1	0	123	227	0	0	227	No
Exon 21	c.3517 G/A	p. 1173 Ala/Thr	115	7	0	122	211	9	0	220	Moessner *et al.* (2007)
Exon 21	c.3788 G/T	p. 1263 Pro/Leu	122	1	0	123	223	3	0	226	Moessner *et al.* (2007)
Exon 21	c.4446 G/A		106	6	0	112	188	14	0	202	No
Exon 22	c.4908 C/T		121	1	0	122	220	0	0	220	No
Exon 22	c.4935 C/T		119	3	0	122	219	2	0	221	No
Exon 22	c.4948 ins/GGCCCC	p.1650 ins. GP	121	1	0	122	222	2	0	224	No

Exon numbering and cDNA sequence are according to the accession no. AB569469 in the DNA Data Bank of Japan.
ASD, autism spectrum disorder; mu, mutation.

skills. His psychomotor development was delayed. The G-banded karyotype (46,XY) was normal, but an EEG showed epileptic discharges. The deletion was inherited from his mother, who is normal. We confirmed the insertion and deletion of a repeated 10-bp GC sequence by polyacrylamide gel electrophoresis and using *Apa*I-digested genome PCR product (Fig. 1e). Interestingly, insertion and deletion were located within an intragenic CpG island (Ching *et al.*, 2007). DNA methylation at CpG dinucleotides is a post replication event that is essential for a properly functioning genome (Lorincz *et al.*, 2004). As a recent study showed that DNA methylation within the CpG island that includes intron 11 regulates intragenic promoter activity and plays an important role in the expression of alternative transcripts in a tissue-specific and cell type-specific manner (Maunakea *et al.*, 2010), alternative transcripts may be aberrantly expressed in the brain tissue of the patient, and further study will be needed.

In addition, a novel heterozygous insertion variant (insertion of two amino acids, glycine and prorine, at 1652) and three reported missense variants (I245T, A1173T, and P1263L) were found in both patient and control samples. We also found five novel synonymous variants (750C/T, 1563G/A, 4446G/A, 4908C/T, and 4935C/T), and two reported variants (483C/T and I245T), in the exons of the *SHANK3* gene. All variants were summarized in Table 1.

Acknowledgements

Grant information: this study was supported by a grant from the Ministry of Education, Culture, Sports and Science and Technology of Japan, and a grant from the Ministry of Health, Labor and Welfare of Japan.

References

Beri S, Tonna N, Menozzi G, Bonaglia MC, Sala C, Giorda R (2007). DNA methylation regulates tissue-specific expression of Shank3. *J Neurochem* **101**:1380–1391.

Böckers TM, Bockmann J, Kreutz MR, Gundelfinger ED (2002). ProSAP/Shank proteins: a family of higher order organizing molecules of the postsynaptic density with an emerging role in human neurological disease. *J Neurochem* **81**:903–910.

Bonaglia MC, Giorda R, Borgatti R, Felisari G, Gangliardi C, Selicorni A, *et al.* (2001). Disruption of the *ProSAP2* gene in a t(12;22)(Q24.1;Q13.3) is associated with the 22q13.3 deletion syndrome. *Am J Hum Genet* **69**:261–268.

Bonaglia MC, Giorda R, Mani E, Aceti G, Anderlid B-M, Baroncini A, *et al.* (2006). Identification of a recurrent breakpoint within the SHANK3 gene in the 22q13.3 deletion syndrome. *J Med Genet* **43**:822–828.

Ching T-T, Manuakea AK, Jun P, Hon C, Zardo G, Pinkel D, *et al.* (2007). Epigenome analyses using BAC microarrays identify evolutionary conservation of tissue-specific methylation of SHANK3. *Nat Genet* **37**:645–651.

Durand CM, Betancur C, Boeckers TM, Bockmann J, Chaste P, Fauchereau F, *et al.* (2007). Mutations in the gene encoding the synaptic scaffolding protein SHANK3 are associated with autism spectrum disorders. *Nat Genet* **39**:25–27.

Gauthier J, Spiegelman D, Piton A, Lafreniere RG, Laurent S, St-Onge J, *et al.* (2008). Novel de-novo SHANK3 mutation in autistic patients. *Am J Med Genet B* **150B**:421–424.

Lim S, Naisbitt S, Yoon J, Hwang J-I, Suh P-G, Sheng M, *et al.* (1999). Characterization of the Shank family of synaptic proteins. Multiple genes, alternative splicing, and differential expression in brain and development. *J Biol Chem* **274**:29510–29518.

Lorincz MC, Dickerson DR, Schmitt M, Groudine M (2004). Intragenic DNA methylation alters chromatin structure and elongation efficiency in mammalian cells. *Nat Struct Mol Biol* **11**:1068–1075.

Manning MA, Cassidy SB, Clericuzio C, Cherry AM, Schwartz S, Hudgins L, *et al.* (2004). Terminal 22q deletion syndrome: a newly recognized cause of speech and language disability in the autism spectrum. *Pediatrics* **114**:451–457.

Maunakea AK, Nagarajan RP, Bilenky M, Ballinger TJ, D'Souza C, Fouse SD, *et al.* (2010). Conserved role of intragenic DNA methylation in regulating alternative promoters. *Nature* **466**:253–257.

Moessner R, Marshall CR, Sutcliffe JS, Skaug J, Pinto D, Vincent J, *et al.* (2007). Contribution of SHANK3 mutations to autism spectrum disorder. *Am J Hum Genet* **81**:1289–1297.

Naisbitt S, Kim E, Tu JC, Xiao B, Sala C, Valtschanoff J, *et al.* (1999). Shank, a novel family of postsynaptic density proteins that binds to the NMDA receptor/PSD-95/GKAP complex and cortactin. *Neuron* **23**:569–582.

Phelan MC, Rogers RC, Saul RA, Stapleton GA, Sweet K, McDermid H, *et al.* (2001). 22q13 deletion syndrome. *Am J Med Genet* **101**:91–99.

Sheng M, Kim E (2000). The Shank family of scaffold proteins. *J Cell Sci* **113**:1851–1856.

Tanaka N, Goto Y, Akanuma J, Kato M, Kinoshita T, Yamashita F, *et al.* (2010). Mitochondrial DNA variants in a Japanese population of patients with Alzheimer's disease. *Mitochondrion* **10**:32–37.

Uchino S, Wada H, Honda S, Nakamura Y, Ondo Y, Uchiyama T, *et al.* (2006). Direct interaction of postsynaptic density-95/Dlg/ZO-1 domain-containing synaptic molecule Shank3 with GluR1 α-amino-3-hydroxy-5-methyl-4-isoxazole propionic acid receptor. *J Neurochem* **97**:1203–1214.

Wilson HL, Wong ACC, Shaw SR, Tse W-Y, Stapleton GA, Phelan MC, *et al.* (2003). Molecular characterization of the 22q13 deletion syndrome supports the role of haploinsufficiency of SHANK3/PROSAP2 in the major neurological symptoms. *J Med Genet* **40**:575–584.

Kondo et al. Molecular Brain 2011, 4:27
http://www.molecularbrain.com/content/4/1/27

Molecular Brain

RESEARCH Open Access

Long-term changes of spine dynamics and microglia after transient peripheral immune response triggered by LPS *in vivo*

Satoru Kondo[1*], Shinichi Kohsaka[2] and Shigeo Okabe[1]

Abstract

Background: An episode of peripheral immune response may create long-lasting alterations in the neural network. Recent studies indicate a glial involvement in synaptic remodeling. Therefore it is postulated that both synaptic and glial changes could occur under the peripheral inflammation.

Results: We tested this possibility by *in vivo* two-photon microscopy of dendritic spines after induction of a peripheral immune response by lipopolysaccharide (LPS) treatment of mice.
We observed that the spines were less stable in LPS-treated mice. The accumulation of spine changes gradually progressed and remained low over a week after LPS treatment but became significantly larger at four weeks. Over eight weeks after LPS treatment, the fraction of eliminated spines amounted to 20% of the initial population and this persistent destabilization resulted in a reduction of the total spine density.
We next evaluated glial activation by LPS administration. Activation of microglia was confirmed by a persistent increase of Iba1 immunoreactivity. Morphological changes in microglia were observed two days after LPS administration and were partially recovered within one week but sustained over a long time period.

Conclusions: These results indicate long-lasting aggravating effects of a single transient peripheral immune response on both spines and microglia. The parallel persistent alterations of both spine turnover and the state of microglia *in vivo* suggest the presence of a pathological mechanism that sustains the enhanced remodeling of neural networks weeks after peripheral immune responses. This pathological mechanism may also underlie long-lasting cognitive dysfunctions after septic encephalopathy in human patients.

Keywords: Peripheral inflammation, Spine, Microglia, *in vivo* imaging, Sepsis

Background

Sepsis is a serious medical condition caused by a severe immune response to infection. Recent studies have demonstrated that patients recovered from septic conditions can have long-term cognitive impairment, including memory deficits and attention disorders [1]. How impairment of brain functions persists long after recovery from sepsis still remains to be poorly understood. Peripheral injection of bacterial lipopolysaccharide (LPS), endotoxin from gram-negative bacteria, mimics the pathological state of sepsis. LPS interacts with Toll-like receptors on macrophages and initiates production of a variety of proinflammatory cytokines including tumor necrosis factor (TNF)- α, interleukin (IL)-1β, and IL-6 [2,3]. These cytokines cross the blood-brain barrier, activate cells of the brain capillaries, and also activate vagal afferents. Subsequently, these responses further induce the synthesis of prostaglandins [4-6] and cytokines within the brain that cause fever and general feelings of illness [7].

Consistent with cognitive impairment in human subjects who recovered from sepsis, peripheral administration of LPS in rodents has been shown to affect cognitive functions [8]. In line with these findings, LPS has also been demonstrated to impair long-term potentiation (LTP), a key cellular process in learning and memory

* Correspondence: kondo@med.kyushu-u.ac.jp
[1]Department of Cellular Neurobiology, Graduate School of Medicine, University of Tokyo, Bunkyo-ku, Tokyo 113-0033, Japan
Full list of author information is available at the end of the article

[9,10]. How does LPS-evoked peripheral inflammation affect functions of the neural network? One obvious possibility is through alterations of glia [11]. Microglial cells are resident immune cells in the CNS [12,13] and have the ability to respond to inflammation by changing their shape from ramified to amoeboid morphology [14] or by changing the expression profile of marker molecules, such as ionized calcium binding adaptor molecule 1 (Iba1) [15,16]. Recent *in vivo* imaging studies reported rapid motility of microglial processes [17,18]. Direct contact of microglia with synapses may also be involved in synapse stripping in pathological conditions [19].

The neuronal network in the mammalian forebrain has been shown to be intrinsically dynamic [20,21] and *in vivo* time-lapse two-photon microscopy of dendritic spines in the mouse neocortex has provided direct evidence of network remodeling [22,23]. Although previous *in vivo* imaging studies reported remodeling of synapses after induction of ischemia [24,25] and in neurodegenerative conditions [26,27], long-lasting changes of synapses triggered by peripheral inflammatory responses have not yet been investigated. Here we performed *in vivo* spine imaging after LPS treatment. Surprisingly, mild and transient peripheral inflammation induced long-lasting changes of spine dynamics, associated with persistent up-regulation of Iba1 expression in microglia. The parallel sustained alterations of both spine turnover and the state of microglia *in vivo* may underlie long-term cognitive impairment after septic encephalopathy in human patients.

Methods

Animals

All experimental procedures were carried out in compliance with the institutional guidelines of the University of Tokyo and the government. This study was approved by the animal welfare ethics committee at the University of Tokyo, Faculty of Medicine with the approval ID of P08-016. Every effort was made to minimize the suffering and the number of animals used.

For *in vivo* imaging and histochemical analyses, both male and female C57BL/6 transgenic mice aged two to three months were used. For *in vivo* spine imaging, transgenic mice expressing green fluorescence protein (GFP) under the control of the *Thy1* promoter (*Thy1-GFP* M mice) were used [28]. To visualize microglia, transgenic mice expressing GFP under the control of the *Iba1* promoter (*Iba1-GFP* mice) were used [29].

Drug treatment

E.coli lipopolysaccharide (LPS, strain O111:B4, Sigma-Aldrich (catalog number L4391)) was dissolved in a saline solution at a concentration of 0.2 mg/mL and stored at -30°C in small aliquots. Mice were intraperitoneally injected with a single dose of LPS (0.5 mg/kg). The optimal dose of LPS was determined from the morphological changes in microglia two days after LPS injection with doses of 0.1, 0.3, 0.5 or 5.0 mg/kg. We observed morphological changes in microglia at doses higher than 0.5 mg/kg. Injection of LPS at 5.0 mg/kg induced severe behavioral responses, while sickness behavior was less prominent at lower doses. From these pilot experiments, we selected a dose of 0.5 mg/kg for experiments with spine imaging and glial activation.

Surgery

Mice were deeply anesthetized intraperitoneally with ketamine (100 mg/kg body weight) and xylazine (10 mg/kg body weight) diluted in a saline solution. After the disappearance of the pinching response the hair of the scalp was shaved and a midline incision of the scalp was made. Periosteum tissue was removed with a surgical blade and the somatosensory area (-1.5 mm from Bregma and 2.0 mm from the midline) was marked by stereotactic coordinates. A small rectangular metal plate with a round hole was glued on the skull and mice were fixed to the immobilized stage (SR-5M, Narishige) with a heating pad to maintain body temperature. The skull above the imaging area was thinned through the round hole of the metal plate. The thinning was initially done over a small area (a 1.5 × 1.5 mm square) with a high speed micro-drill (KM11, Minimo). When the bone reached ~50 μm in thickness, further thinning was performed manually with micro surgical blades (NORDLAND blade, Salvin Dental) until the skull reached ~15 μm in thickness. We paid particular attention not to push the skull during the thinning process. The final imaging window was a 0.5 × 0.5 mm square. For the repetitive imaging, the brain vasculature pattern was recorded with a CCD camera (GZ-MG70, Victor).

In vivo imaging

A scanning microscope (FV-300, Olympus) equipped with a pulsed laser (MaiTai HP, Spectra Physics) was used for imaging with a water immersion objective lens (1.05 NA, 25x, Olympus). The wavelength was 920 nm and the average power of the laser after the objective lens was between 10 and 20 mW. The imaging area was 234 μm × 234 μm (low magnification) or 78 μm × 78 μm (high magnification), with an imaging depth 50 μm from the surface of the neocortex (Layer 1) and the step size of the z stack set to 0.75 μm. The pixel sizes of single horizontal images were set to 512 × 512. Low magnification images, together with images of the vasculature pattern taken with a CCD camera, served as the reference maps for repetitive acquisition of higher magnification images from the same cortical area. For

repeated imaging, the metal plate attached on the skull was removed and the skin was sutured. The mice were kept on the heating pad until they recovered from the anesthesia and were returned to their home cage. To minimize the damage to the brain tissue due to the re-thinning of the skull, mice were imaged twice for most of the experiments and three times at the maximum.

Fixation of animals and immunohistochemistry

Wild type or *Iba1-GFP* mice were sampled before or two, seven, 28 days after LPS injection. Mice were deeply anesthetized with pentobarbital and perfused transcardially with PBS followed by 4% paraformaldehyde. Brains were removed and further fixed in 4% paraformaldehyde overnight at 4°C. Slices were made with a vibratome (DTK-1000, Dosaka EM) with a 50 μm thickness. Slices from wild type mice were stained with anti-Iba1 antibody (1/500, Wako Pure Chemicals) or anti-glial fibrillary acidic protein (GFAP) antibody (1/3000, Sigma-Aldrich) followed by the fluorescence conjugated secondary antibodies to visualize the microglia or astrocytes. Mice from various time intervals after LPS injection or control were fixed on the same day and slices were stained at the same time. Images were obtained by using a laser scanning confocal microscope (FV-1000, Olympus) or a wide-field fluorescence microscope (BX-50, Olympus) under the same illumination and collection conditions.

Data analysis

All analyses of spine dynamics, densities, and estimations of sizes were done manually using National Institutes of Health ImageJ software (http://rsb.info.nih.gov/ij). We could identify both spines and filopodia [30] but analyzed only dendritic protrusions classified as spines in this study (Figure 1) [31]. The same dendritic segments (5-50 μm length) were identified from the image stacks at different time points and spines were selected and classified into three groups. New spines were those identified only at the second time point. Eliminated spines were those present only at the first time point but missing at later points. Spines present at both time points were categorized as stable spines. The number of spines in each group was counted and both the formation and elimination rates were calculated as the percentages of eliminated spines and newly formed spines to the total number of spines examined respectively. To ensure the tissue movements and rotations three-dimensional stacks were always used for the analysis. We did not analyze structures that projected mainly along the imaging axis, below or above dendrites. We considered a spine in the second image to be the same spine as in the first image if the second image spine was located within 0.5 μm of the expected location based on its spatial relationship to adjacent spines or landmarks like axonal and dendritic orientation.

For the morphological analysis of spines, we selected dendritic segments where eliminated spines could be identified. Binary images were constructed by appropriate thresholding to determine the outline of spines. The length from the neck to the tip of a spine (a) and the maximum width of a head (b) were measured manually and the sum of these two values was taken as a parameter reflecting spine size.

For the spine density analysis, we used the same dendritic segments as in the spine turnover analysis. We selected the dendritic segments whose lengths were more than 20 μm for the spine density calculation. Spine density was calculated as (N of spines)/(lengths of dendritic segments).

For the analysis of Iba1 expression we took 41 images at the z step of 1 μm and a maximum projection image was generated from the same number of stack images for all the individual slices. Images were obtained with a laser scanning confocal microscope (FV-1000, Olympus) under the same illumination and collection conditions. The total fluorescence intensity of projection image was measured by ImageJ software. The background intensity was subtracted from the total fluorescence intensity. The intensity values were normalized to the mean intensity value of the control.

The density of microglia was calculated from the same slices as used for the measurement of intensity. The number of Iba1-positive cell bodies was manually counted three-dimensionally from 41 image stacks. The number of microglia was normalized to the mean number of microglia in the control.

Imaris v6.1.3 (Bitplane, Zurich, Switzerland) was used for the three-dimensional analysis of microglial processes. Surface rendering of GFP-positive microglia from z-stacks of confocal microscope images was performed and the lengths of processes were determined by measuring the distance from the centroid of a cell body to the tip along the processes.

Structural dynamics of microglia were quantified from time-lapse imaging of soma and protrusions *in vivo*. Images were obtained every three min for 30 min. We took 51 images at the z step of one μm for each time-interval image. The analysis was performed on maximum-intensity projections of fluorescence image stacks. The same number of stack images was used for each cell analysis. The dynamics of microglia were evaluated by measuring the length of extension and retraction of microglial protrusions. Ten processes of microglia were randomly selected and the length of extension and retraction was measured to compare the overlay of two images at two different time points.

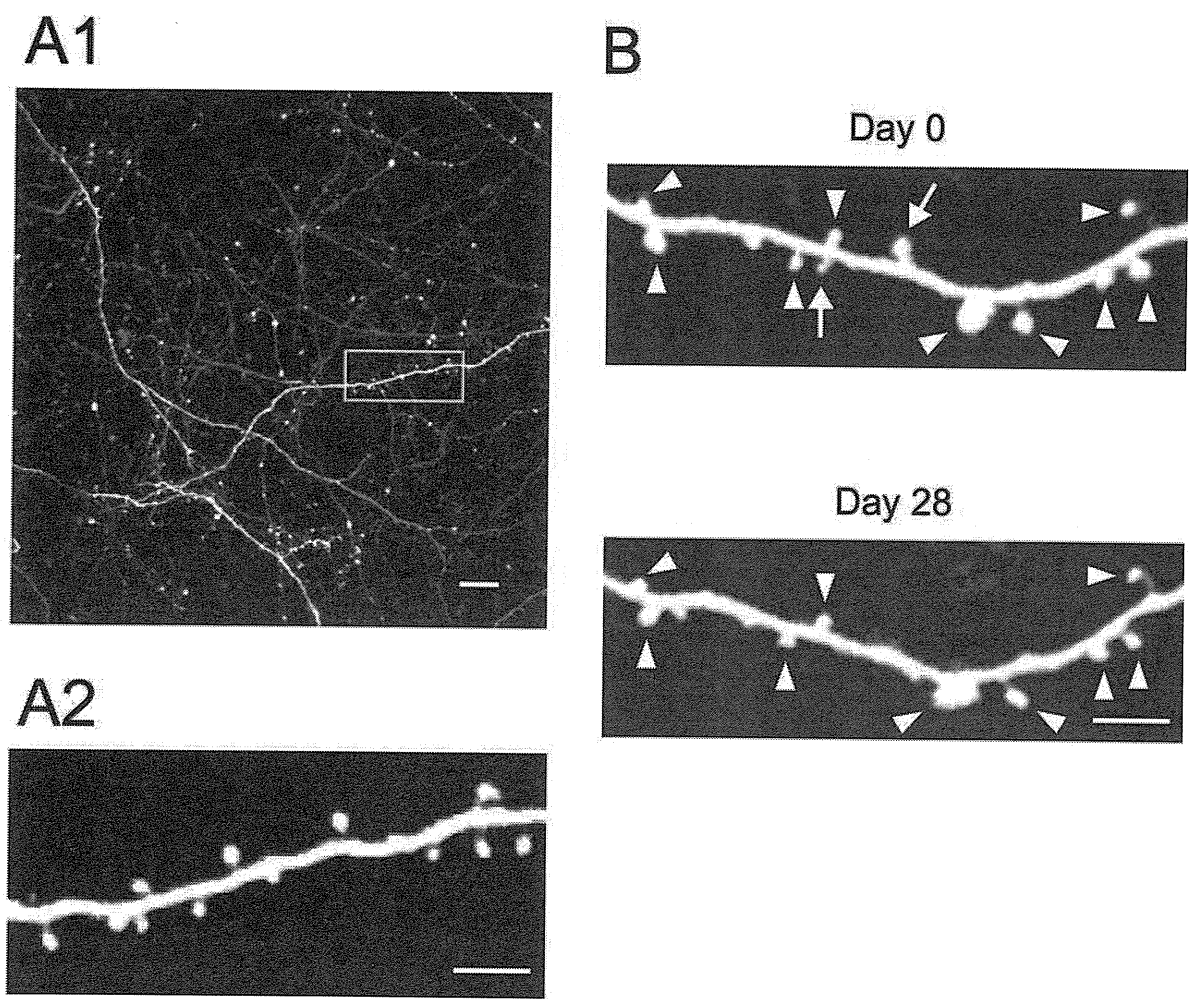

Figure 1 Two-photon microscopy of dendritic spines. (A1) Typical morphologies of dendrites in the superficial layer of the neocortex detected by *in vivo* two-photon microscopy. This is a projection image of z-stacks. Scale bar, 10 μm. (A2) Higher magnification view of the dendritic segment marked by the rectangle in A1. The image was generated from a montage of several adjacent optical sections separated by 0.75 μm in the Z-direction. Scale bar, 5 μm. (B) *In vivo* imaging of dendritic segments at two time points (day 0 and day 28). These images were also generated from a montage of several adjacent optical sections separated by 0.75 μm in z-direction, illustrating stable spines (arrowheads) and eliminated spines (arrows). Scale bar, 5 μm.

All the data are presented as means ± S.D. Multiple comparisons were made by an ANOVA test, followed by a Tukey's test (Figures 2, 3, 5, 6, 7). Statistical significance was evaluated using Student's t-test (Figure 4). Differences were considered to be significant if $p < 0.05$.

Cytokine array analysis

Tissue extracts from control and LPS-treated mice were screened by using a cytokine antibody array kit (Array1, RayBiotech Inc., Atlanta, GA, USA) according to the manufacturer's instructions. After euthanasia of mice with a large dose of pentobarbital, the neocortex and the hippocampus were dissected from the forebrain and homogenized in a lysis buffer. Brain extracts were then centrifuged at 10,000 × g for 10 min at 4°C. Protein concentrations of supernatants were determined and equal amounts of protein were incubated with array membranes. The signals generated by enhanced chemiluminescence were recorded by ChemiDoc XRS (Bio-Rad, Tokyo, Japan). For the analysis of chemiluminescence signals from cytokine spots, total signals were calculated and then background intensity was subtracted. The averaged optical densities of the six positive controls on the membrane were calculated and the optical densities of cytokine spots were divided by these values. These normalized values were compared and the ratio between control and LPS-treated mice was calculated.

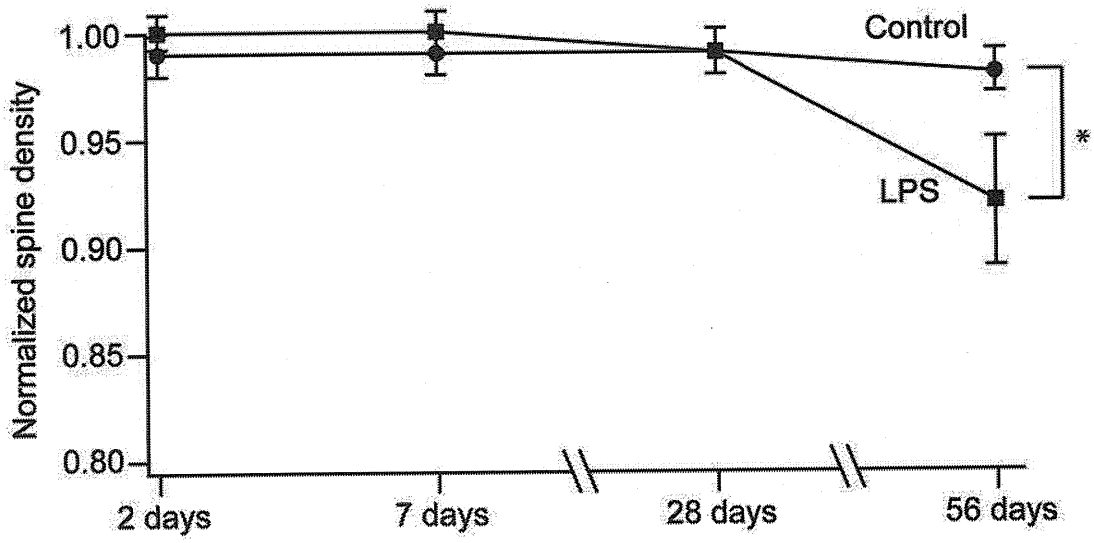

Figure 2 Temporal change of spine density after LPS treatment. Average spine densities at different time points after LPS treatment were calculated and normalized against the value at day zero (before LPS administration in the LPS-treated group). Spine densities were maintained close to the original value until 28 days after LPS injection. However, there was a late decline of spine density in LPS-treated group and the difference was statistically significant (*, $p < 0.05$).

Results

Transient peripheral immune response induces long-lasting changes of spine dynamics *in vivo*

Turnover of excitatory synapses in the neocortex with or without stimulation of the peripheral immune system can be quantitatively evaluated by two-photon imaging of dendritic spines *in vivo*. We visualized apical dendrites of pyramidal neurons in the somatosensory cortex of adult transgenic mice expressing GFP under the control of the *Thy1* promoter in a small subset of the CNS neurons (*Thy1-GFP* M mice) [28]. We selected the thinned-skull method in this study, because of the less prominent effects of this surgical procedure on the activation of glial cells [32]. To detect spines generated and eliminated, we obtained image stacks of GFP-filled dendrites by two-photon microscopy at two time points separated by two days, seven days, four weeks or eight weeks (Figure 1A). A pair of image stacks was compared and spines present in both image stacks, and those present only at a single time point were identified manually (Figure 1B). After identification and classification of spines, the fractions of newly formed spines and eliminated spines were calculated. The fraction of spines added or eliminated in unperturbed animals was low and comparable to a previous report [33]. The fraction of dynamic spines was less than 5% over a period of seven days, 5% over four weeks, and still less than 10% over a period of eight weeks (see Figure 3B).

We challenged *Thy1-GFP* M mice with peripheral administration of LPS and measured the turnover rate of spines. The dose of LPS (0.5 mg/kg) was set to the minimal dose sufficient for up-regulation of Iba-1, which is a well-characterized marker of microglial activation. The protocols for imaging were set to be identical for control and LPS-treated groups, except that the LPS-treated group received a single intraperitoneal injection of LPS after acquisition of spine images on the first day. We first determined if there were any alterations in spine densities after LPS administration (Figure 2). Spine densities (estimated from images taken over intervals from two days to four weeks within the same volume of the cortex) did not show prominent differences, with a tendency for a slight decline [33,34]. However, there was a significant reduction in spine density at eight weeks after LPS treatment, indicating a late impact of LPS treatment on the cortical network.

Delayed changes in the total spine density may be derived from persistent changes in the spine addition/elimination rates triggered by LPS. To test this possibility, we calculated the fractions of added or eliminated spines (Figure 3A). Within the first week after LPS treatment, these dynamic fractions were not significantly larger than the corresponding fractions in the control group (Figure 3B). However, when we waited for four weeks, the fractions of added or eliminated spines accumulated after LPS treatment were significantly larger than the corresponding fractions in the control group (5.5% (control) versus 11.0% (LPS-treated) for spine elimination, 5.2% (control) versus 10.7% (LPS-treated) for spine formation at four weeks). Spine elimination was further enhanced by LPS treatment when we waited for eight weeks (7.2% (control) versus 20.9%

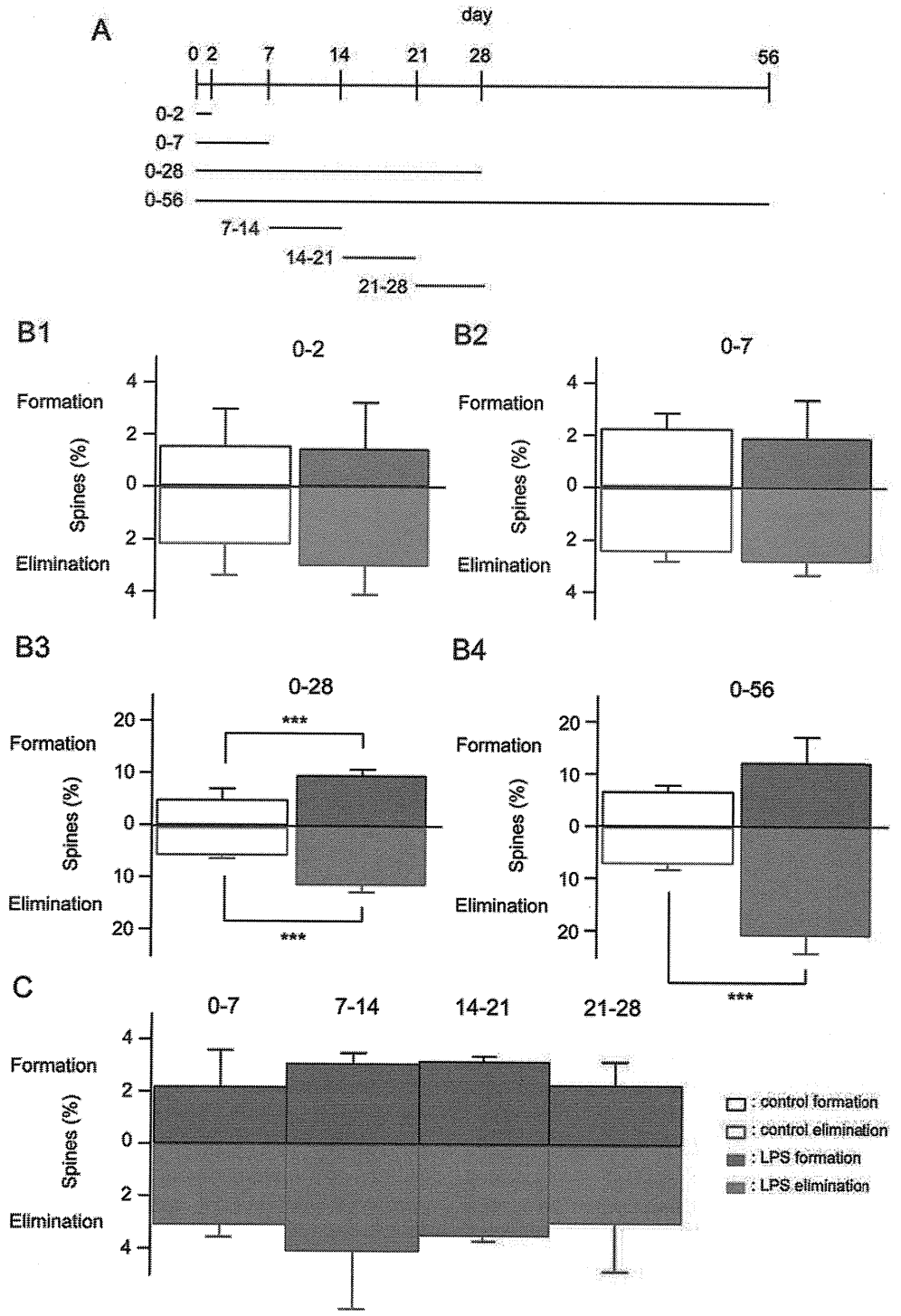

Figure 3 Persistent up-regulation of spine turnover in mice treated with LPS. (A) Spine turnover rates were measured as illustrated in the scheme. (B) Spine turnover rates of control and LPS-treated mice measured at two, seven, 28, and 56 days. Upward bars (black) and downward bars (red) represent the formation and elimination rate of spines, respectively. Spines formed and eliminated in control: 2.4 ± 1.4% and 2.5 ± 1.1% over two days (N = 6) (B1), 2.6 ± 0.4% and 2.7 ± 0.6% over seven days (N = 6) (B2), 5.2 ± 2.1% and 5.5 ± 0.6% over 28 days (N = 6) (B3), 6.8 ± 1.1% and 7.2 ± 1.1% over 56 days (N = 3) (B4). Spines formed and eliminated after LPS injection: 1.7 ± 1.8% and 3.3 ± 1.1% over two days (N = 3) (B1), 2.2 ± 1.4% and 3.1 ± 0.5% over seven days (N = 3) (B2), 10.7 ± 1.5% and 11.0 ± 1.2% over 28 days (N = 6) (B3), 12.4 ± 4.9% and 20.9 ± 3.5% over 56 days (N = 4) (B4). These data were statistically compared between control and LPS treatment (spines formed: $p > 0.5$ for two days; $p > 0.5$ for seven days; $p < 0.001$ for 28 days; $p > 0.1$ for 56 days; spines eliminated: $p > 0.1$ for two days; $p > 0.1$ for seven days; $p < 0.001$ for 28 days; $p < 0.001$ for 56 days). ***, $p < 0.001$. (C) Spine turnover measured with a fixed interval but with different days of the first imaging.

(LPS-treated)), but the extent of spine addition did not match that of elimination in the LPS-treated group (6.8% (control) versus 12.4% (LPS-treated)). This unbalance of addition and elimination of spines could explain the reduction of the total spine density at eight weeks after LPS treatment.

The selective increase of the dynamic spine fraction at late time points could be explained by either an accumulation of small changes gradually over time or by abrupt up-regulation of dynamics at specific time points. To discriminate between these two possibilities, we imaged dendritic spines with intervals fixed to one week, but altered the first imaging days to be either zero, seven, 14, or 21 days after LPS treatment. We could not detect up-regulation of spine dynamics in any of these time segments (Figure 3C), supporting the first possibility that the accumulation of small changes only becomes obvious four weeks after LPS treatment. In other words, these results indicate the presence of persistent alterations in spine dynamics lasting well beyond several weeks after transient and mild activation of the peripheral immune system.

Morphological characteristics of eliminated spines

Next, we evaluated morphological characteristics of spines eliminated early (within one week) or late (later than four weeks) after the initial time point of the spine imaging. Previous reports on spine lifetime in slices indicated that spines with larger volumes had longer lifetimes [35]. Therefore, small spines may have a higher probability for elimination after LPS treatment *in vivo*. On the other hand, if spine elimination is a stochastic process with no preference for size, we might not detect any differences in spine size between groups with different lifetimes. To discriminate between these possibilities, we evaluated the morphology of individual spines by calculating the sum of their lengths and widths (Figure 4A). This measurement suggests that indeed there exists differences in morphology between spines eliminated within one week and those that remained (Figure 4B1). Eliminated spines tended to be smaller than the stable ones ($p < 0.001$). However, a similar comparison between spines eliminated within one month and those that survived for one month did not show such a tendency (Figure 4B2). Thus, we consider the spines with a life-time of less than a week morphologically distinct from the remaining spine population.

LPS treatment increased the fraction of added and eliminated spines only in a late phase. At four weeks after LPS treatment, the fraction of eliminated spines was 10%, twice as large as the fraction in the control (5%). If LPS treatment affected a subset of spines, such as those with smaller volumes, we might be able to detect changes in the frequency distribution of spines eliminated late after LPS treatment. However, the morphology of spines eliminated within one week or one month was not significantly different between the LPS-treated group and the control group (Figure 4B and 4C), suggesting that there was no preferential impact of LPS treatment on a subset of spines with a specific morphology.

We conclude that spines destined to be eliminated within a week are smaller than the average in both control and LPS-treated conditions. LPS increased the fraction of spines to be eliminated late after LPS treatment, but the morphological difference of this LPS-sensitive fraction could not be detected by comparison of spine images, indicating that the late effect of LPS is to increase the probability of spine elimination irrespective of the spine size.

LPS-induced alterations in glial properties

The *in vivo* imaging of LPS-treated *Thy1-GFP* M mice indicated the presence of persistent alterations in spine dynamics lasting well beyond several weeks after transient activation of the peripheral immune system. Peripheral immune responses can secondarily induce changes in glial components in the CNS, especially in astrocytes and microglial cells [36,37]. We performed immunohistochemistry of the neocortex two, seven and 28 days after LPS treatment to detect activation of astrocytes and microglial cells. We could not detect up-regulation of the astrocytic marker GFAP. However, Iba1, a marker of microglial activation, was up-regulated at all time points examined ($p < 0.001$ for two, seven, 28 days) (Figure 5A and 5B). Notably, up-regulated Iba1 immunoreactivity was maintained even at 28 days after LPS injection. There was also a specific increase of microglial density at 28 days after LPS treatment ($p < 0.01$) (Figure 5C). These results indicate prolonged activation and late proliferation of microglia following a single peripheral administration of LPS.

Peripheral injection of LPS may induce morphological changes of microglia. To test this possibility, we measured the length of microglial processes using a transgenic mouse line expressing GFP in microglia under the control of the *Iba1* enhancer element (*Iba1-GFP* mice) [29]. Cytoplasmic GFP signals from microglia in *Iba1-GFP* mice reflect cellular morphology more precisely than the immunoreactivity of endogenous Iba1, which may reflect both cell shape and intracellular distribution of the protein. There was a transient shrinkage of microglial processes assessed by GFP signal two days after LPS treatment ($p < 0.001$), but the processes showed re-extension at seven and 28 days after LPS treatment (Figure 6). Consistent with the up-regulation of the endogenous *Iba1* gene, GFP expression under the control of the *Iba1* promoter also increased progressively after LPS treatment.

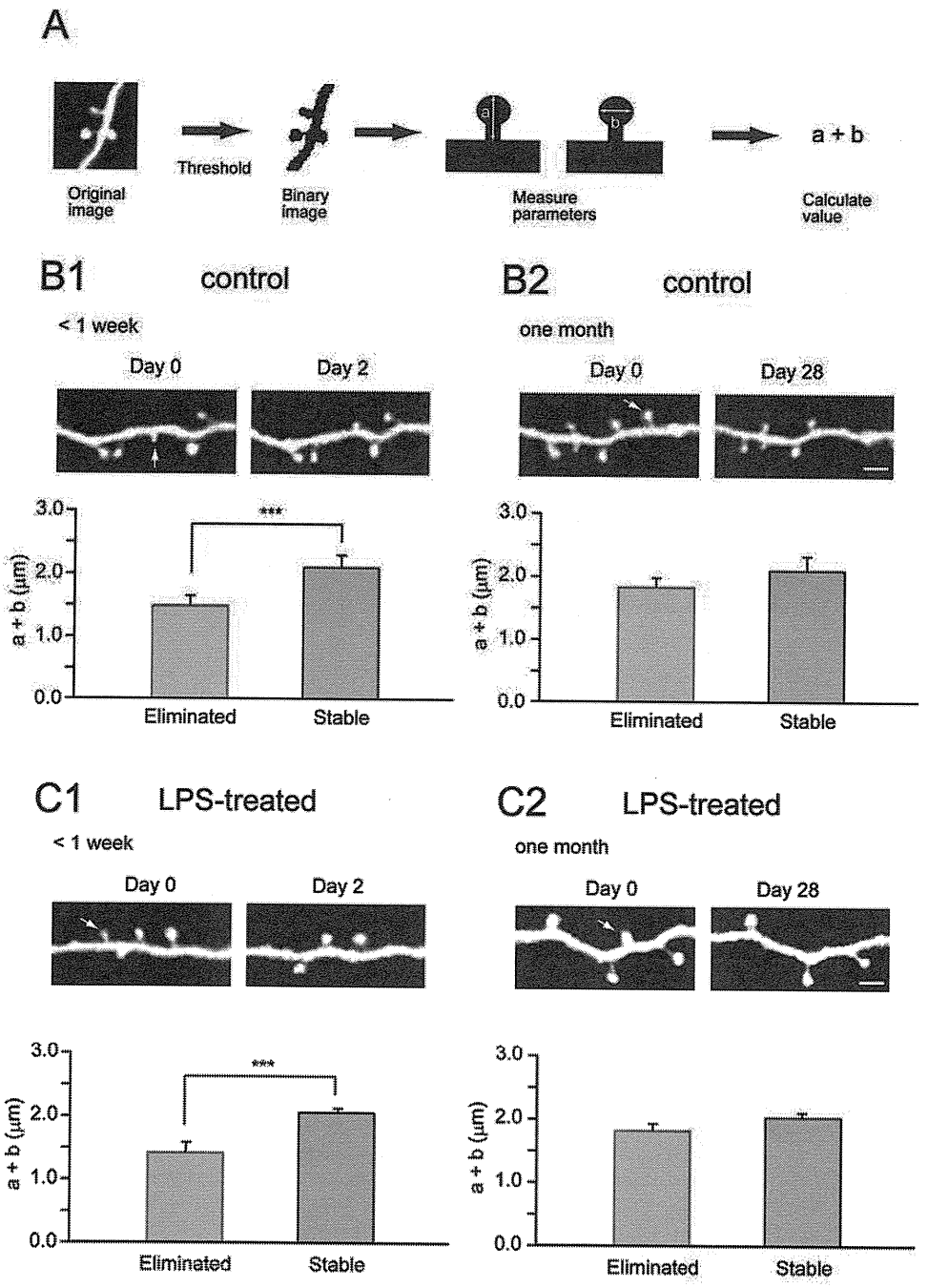

Figure 4 Relationship between spine size and spine elimination. (A) The sizes (both length (a) and width (b)) of spines were measured as illustrated. The sum of the values "a" and "b" was calculated and utilized as an index of spine size. (B1) Spines eliminated within two or seven days were smaller than the spines maintained for the same period. Images are comparisons over two days. An arrow indicates an eliminated spine. The bar graph shows the combined data from images taken over two or seven days, as the frequency distribution of each population was indistinguishable. (B2) When spines were imaged with intervals of 28 days, the sizes of eliminated spines were similar to those of stable spines. An arrow indicates an eliminated spine. (C1) Spines eliminated within two or seven days were smaller than the stable spines also in the LPS-treated group. An arrow indicates an eliminated spine. (C2) Spines eliminated 28 days after LPS treatment had comparable sizes with those maintained. An arrow indicates an eliminated spine. Importantly, the average sizes of eliminated spines between control and LPS-treated groups were not different at two different time points (less than seven days in B1/C1, at 28 days in B2/C2), indicating that the effect of LPS is not selective for a specific size of spines. ***, $p < 0.001$. Scale bars, 2 μm.

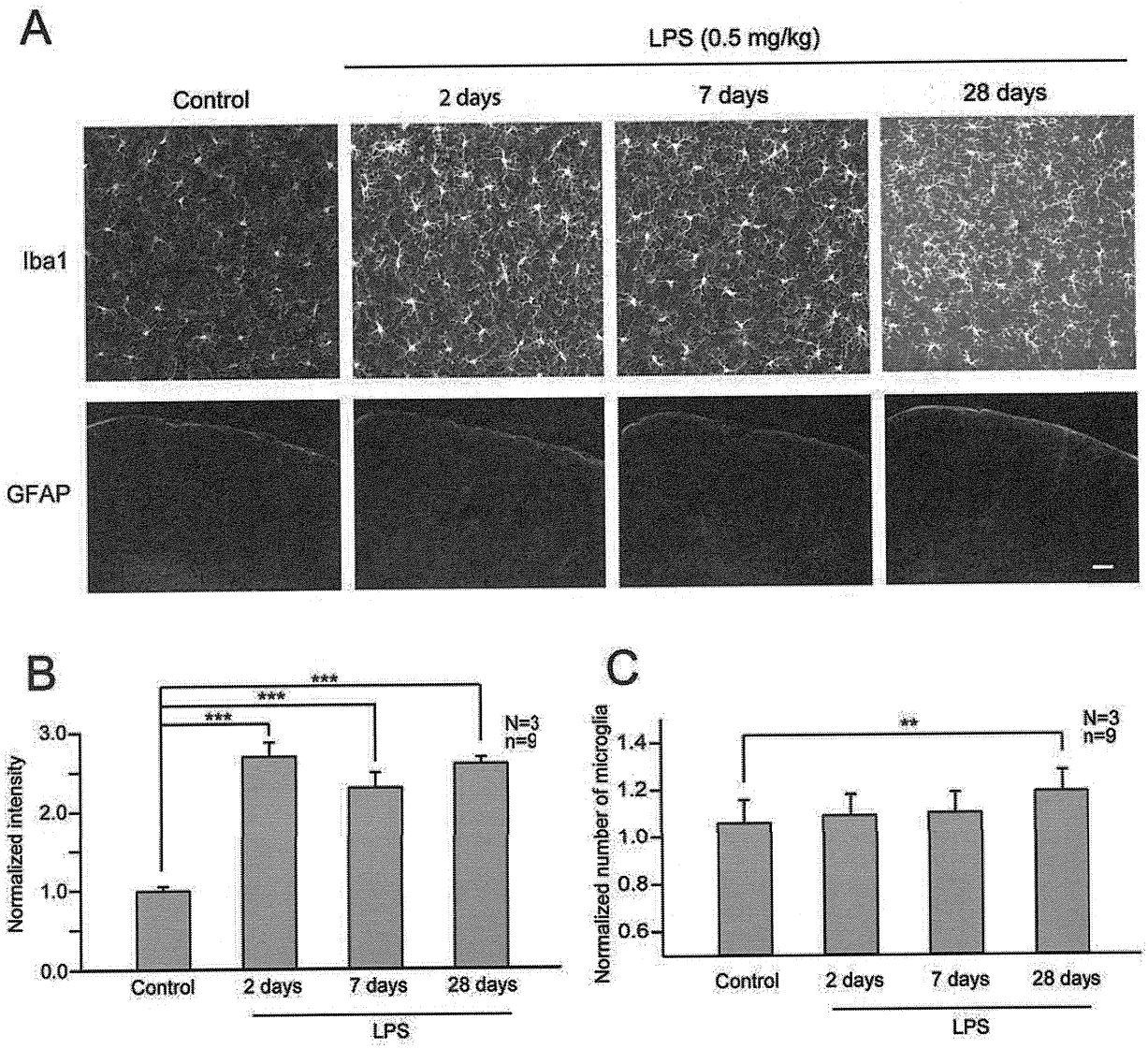

Figure 5 LPS induced persistent activation of microglia. (A) Immunohistochemical analyses were performed with fixed cortical slices from control and LPS treated mice at different time points. Slices were stained either with anti-Iba1 antibody for microglia or anti-GFAP antibody for astrocytes. Projection images are shown. Scale bar in the upper column, 10 μm; bar in the lower column, 400 μm. (B) Temporal profile of enhanced Iba1 expression after LPS treatment. To evaluate expression of Iba1, the total intensity of fluorescence was measured and the averages were plotted as values normalized to the control (N: number of mice, n: number of slices). The intensity of fluorescence was significantly increased after two days of LPS treatment and this increasing trend was maintained until 28 days. (C) Late increase in the number of microglia after LPS treatment. The number of microglia was counted and the averages were plotted as values normalized to the control (N: number of mice, n: number of slices). The number of microglia was significantly increased only at 28 days after LPS treatment. **, $p < 0.01$, ***, $p < 0.001$.

Microglia retracted their processes two days after LPS treatment but recovered from the initial shrinkage of their processes at time points later than seven days. A previous study reported the importance of process motility and contact with synapses for the regulation of synapse remodeling by microglia [19]. To evaluate the extent of microglial process motility, we visualized the dynamics of microglial processes using *in vivo* two-photon microscopy of *Iba1-GFP* mice. Time-lapse images were obtained every three min for 30 min. The temporal profiles of process extension and retraction were created from images of microglia without stimulation (Figure 7A1), microglia two days after LPS treatment (Figure 7A2), and 28 days after LPS treatment (Figure 7A3). The average velocities of process remodeling determined from time-lapse images (Figure 7B) were

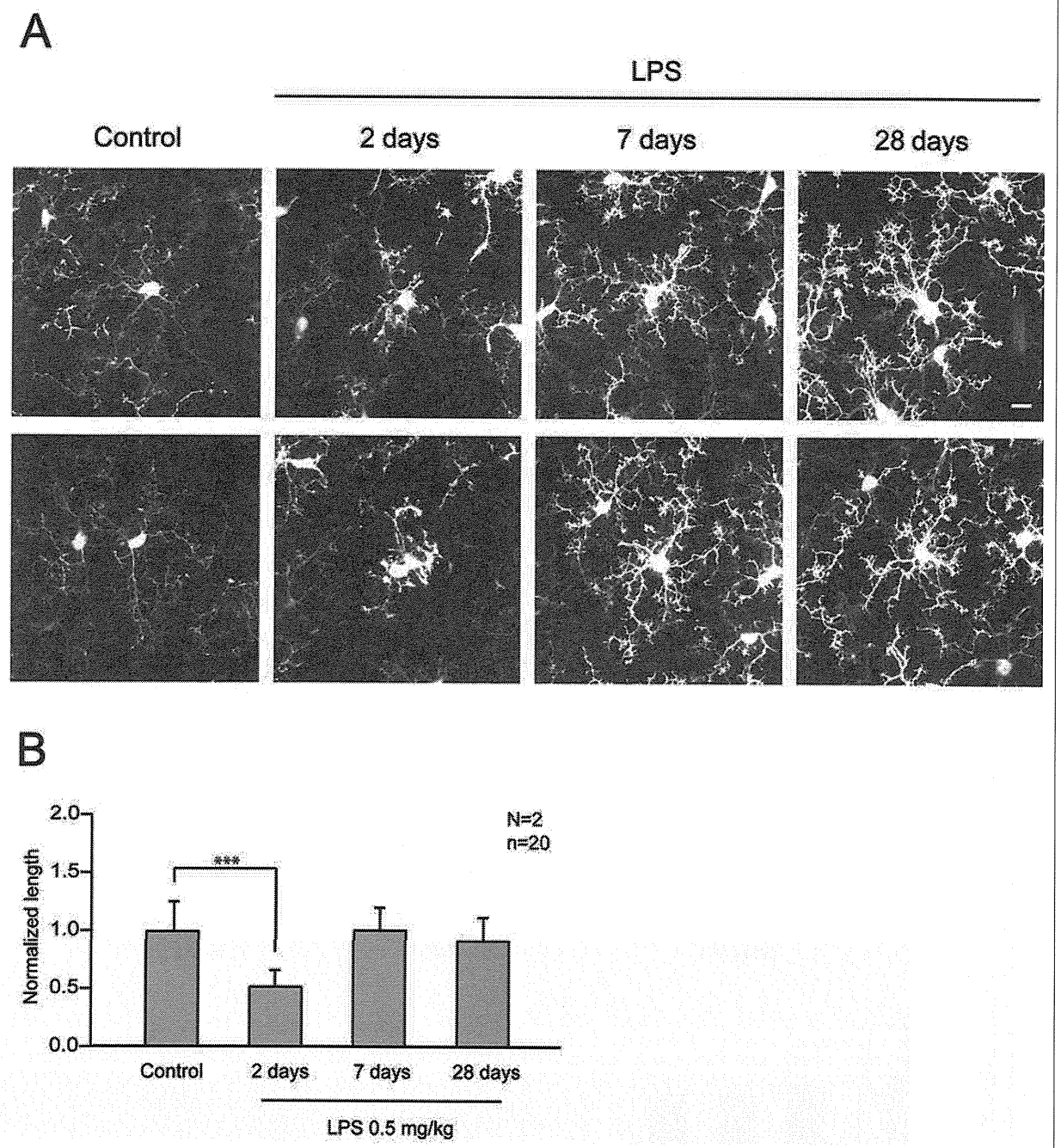

Figure 6 Morphological changes of microglia after LPS treatment. (A) High magnification images of microglia in *Iba1-GFP* mice. Mice were either unperturbed or received LPS injection and were sacrificed for immunohistochemical analyses two, seven, and 28 days later. Scale bar, 10 μm. (B) Total lengths of microglial processes were measured and the averages are shown as lengths normalized to the control (N: number of mice, n: number of microglia). The shrinkage of processes was observed at two days but they recovered their original lengths seven days after LPS injection. GFP signals from the microglial processes were enhanced even at later time points (seven and 28 days), but this may be due to either real increase in process diameters or increases in the GFP protein content. ***, $p < 0.001$.

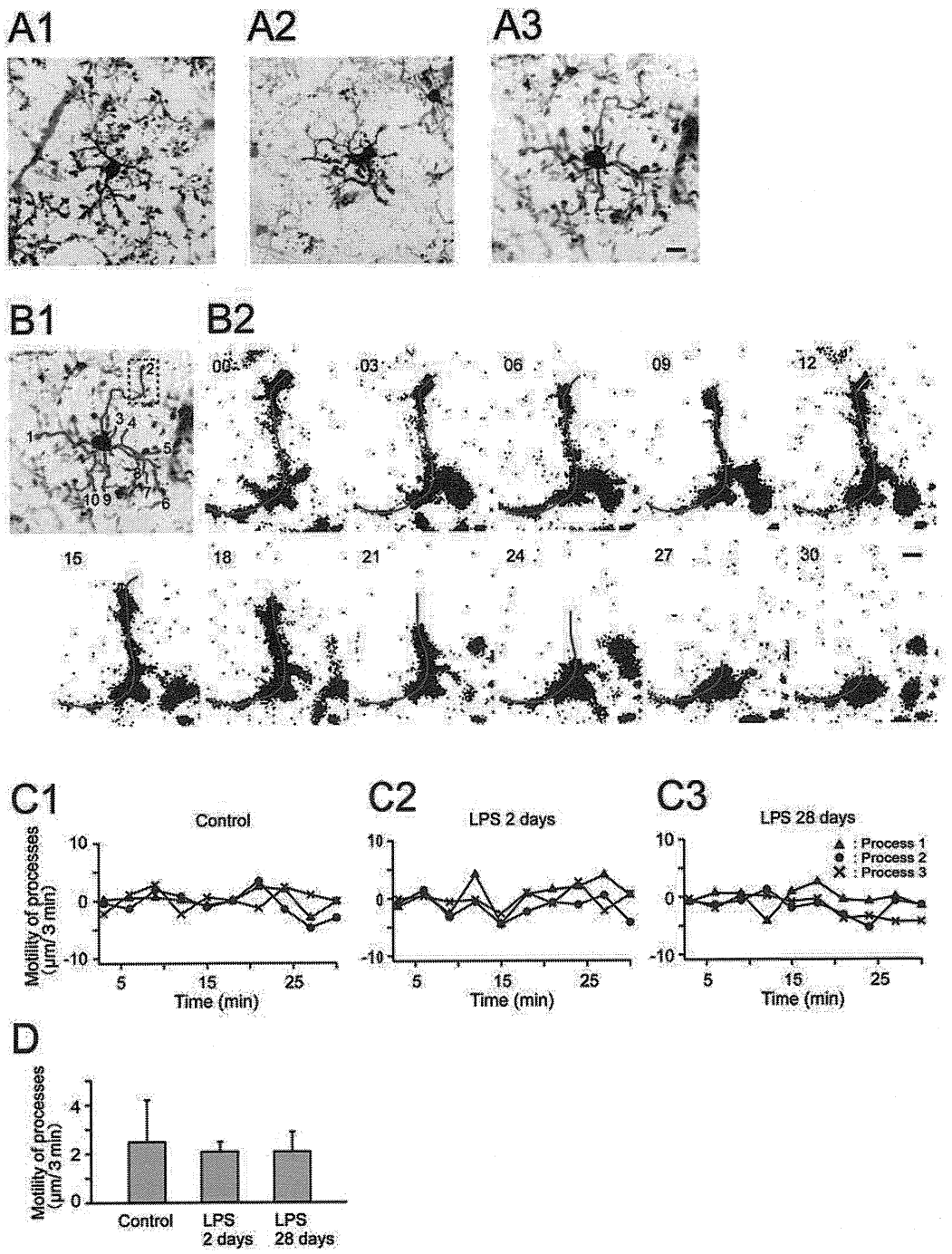

Figure 7 Unaltered dynamics of microglial processes in LPS-treated mice. (A) Morphology of microglia imaged by *in vivo* two-photon microscopy of *Iba1-GFP* mice. A1 shows a cell from a mouse without LPS administration. A2 and A3 show cells from LPS-treated mice at two and 28 days after LPS treatment, respectively. Scale bar, 10 μm. (B1) An example of a microglial cell utilized for time-lapse analysis (identical cell shown in A3). This image shows the morphology at zero time point, with an overlay of green lines (numbered from 1 to 10) on individual processes. The tips of these green lines were recorded and their distances between adjacent time frames (3 min intervals) were calculated as an index of process motility shown in C and D. (B2) Binary images of a microglial process (green line) extracted from time-lapse sequences in the image area marked by a dotted rectangle in B1, illustrating the extent (yellow line) of rapid growth and shrinkage (red line). Numbers in the upper left corner indicate elapsed time in min. Scale bar, 2 μm. (C) The motility of microglial processes. Extension and retraction of processes were plotted for three representative processes with time intervals of three min. Positive values indicate process extension and negative values indicate retraction. (D) Summation of absolute distances of extension and retraction during 30 minutes was calculated and the average speeds per frame (three min) were estimated from 10 processes of control and LPS-treated mice. The average motility was comparable among control and LPS-treated groups.

similar among groups with or without LPS treatment and groups with different intervals between LPS treatment and *in vivo* imaging (Figure 7C and 7D). These observations indicate microglia in both acute and chronic phases after LPS treatment are able to interact with synapses with their highly dynamic processes.

Brain cytokine and chemokine profiles after LPS treatment

We next asked whether soluble factors, such as TNF-α and IL-6, in the neocortex were persistently modulated after LPS treatment. Inflammation induces the expression of a variety of cytokines and chemokines in microglia [38]. Profiles of 22 different cytokines and chemokines in lysates taken from the neocortex of mice were evaluated by using antibody array membranes. We prepared brain lysate from mice sacrificed at multiple time points (one hr, two days, or 28 days) after LPS treatment (N = 1 for one hr and two days (data not shown), N = 3 for 28 days) and from control mice (N = 3). Signals were detected by a chemiluminescence method and were compared with the signal intensity of control mice (Figure 8A and 8B). We did not detect more than a two-fold increase or decrease in the level of cytokines/chemokines tested at any time point (Figure 8C). To test the sensitivity of our membrane array system, we challenged the mice with a ten-fold higher dose of LPS (5 mg/kg) (N = 1) that reportedly induces the amoeboid transformation of microglia and up-regulation of cytokines. In this condition, we successfully detected the up regulation of some cytokines (IL-6, IL-12, and TNF-α; data not shown) as reported previously [37]. This demonstrated that the detection system was indeed capable of measuring marked changes in cytokines/chemokines. Thus, at the LPS dose used in our imaging experiments, spine turnover rate might be modulated by other soluble factors secreted from microglia. However, we can not exclude the possibility that activated microglia, which corresponds to a small fraction of the cells present in the neocortex, secreted factors whose amount is under the limit of sensitivity of our detection system.

Discussion

In this study, we addressed the question of how peripheral immune responses can modulate network remodeling of the neocortex *in vivo*. We imaged dendritic spines *in vivo* and analyzed spine dynamics over a period of several days to weeks after transient activation of the peripheral immune system with LPS. Within a week after LPS treatment, spine dynamics were low and comparable to those in control mice, indicating a minimal acute effect of systemic LPS treatment. Surprisingly, the fraction of newly formed or eliminated spines accumulated during four weeks after LPS treatment was twice as large as the proportion in control mice. The enhanced spine turnover was associated with persistent activation of microglial cells. The persistent modification of both spine dynamics and microglial activity suggests long-lasting effects of a single transient peripheral immune response on brain functions.

Peripheral immune response triggers sustained up-regulation of spine turnover *in vivo*

In vivo imaging of dendritic spines can be achieved by two different surgical techniques. The first approach, using chronic open-skull glass windows, provides clear imaging windows for efficient two-photon excitation in the deeper cortical layers without a limit on imaging time points [31]. The second approach, using thinned skull windows, gives less efficient excitation of the deep cortical layers and is limited in the number of repetitive imaging, due to the technical difficulty of thinning the same cranial tissue multiple times [22]. Previous reports indicate that the open-skull window is associated with transient glial activation, which is not present after proper thinned-skull surgery [32]. Because our research goal was to assess the influence of mild peripheral immune response on the remodeling of the neural network, we had to exclude any possibility of inducing inflammation in the brain parenchyma due to the imaging protocol itself. Therefore, we imaged dendritic spines through a thinned-skull window in this study and successfully confirmed the remarkably stable nature of dendritic spines (turnover of < 10% over one month) [22].

In order to activate the peripheral immune system, we administered a single low dose of LPS intraperitoneally. This treatment induced persistent enhancement of spine turnover in vivo. We used the lowest possible dose of LPS (0.5 mg/kg) to induce up-regulation of Iba-1 immunoreactivity in microglia and there was no sign of acute neuronal degeneration in the brain (data not shown). A previous study by Sparkman *et al.* using a single intraperitoneal injection of LPS at the low dose of 0.25 mg/kg reported the presence of classic signs of sickness behavior, including decreased locomotion, hunched posture, piloerection, and anorexia [39]. Therefore we cannot eliminate the possibility that emotional and cognitive alterations acutely induced by sickness-related behavioral changes are partly responsible for alterations in spine dynamics. On later days of in vivo imaging, however, mice are fully recovered and it is less likely that the initial sickness behavior is the direct cause of the enduring enhancement of spine dynamics. Instead, we propose that persistent activation of microglia over a period of more than several weeks plays an important role in enhanced synapse remodeling.

Synapse formation and elimination are believed to be the basis for the plastic changes of neuronal circuits

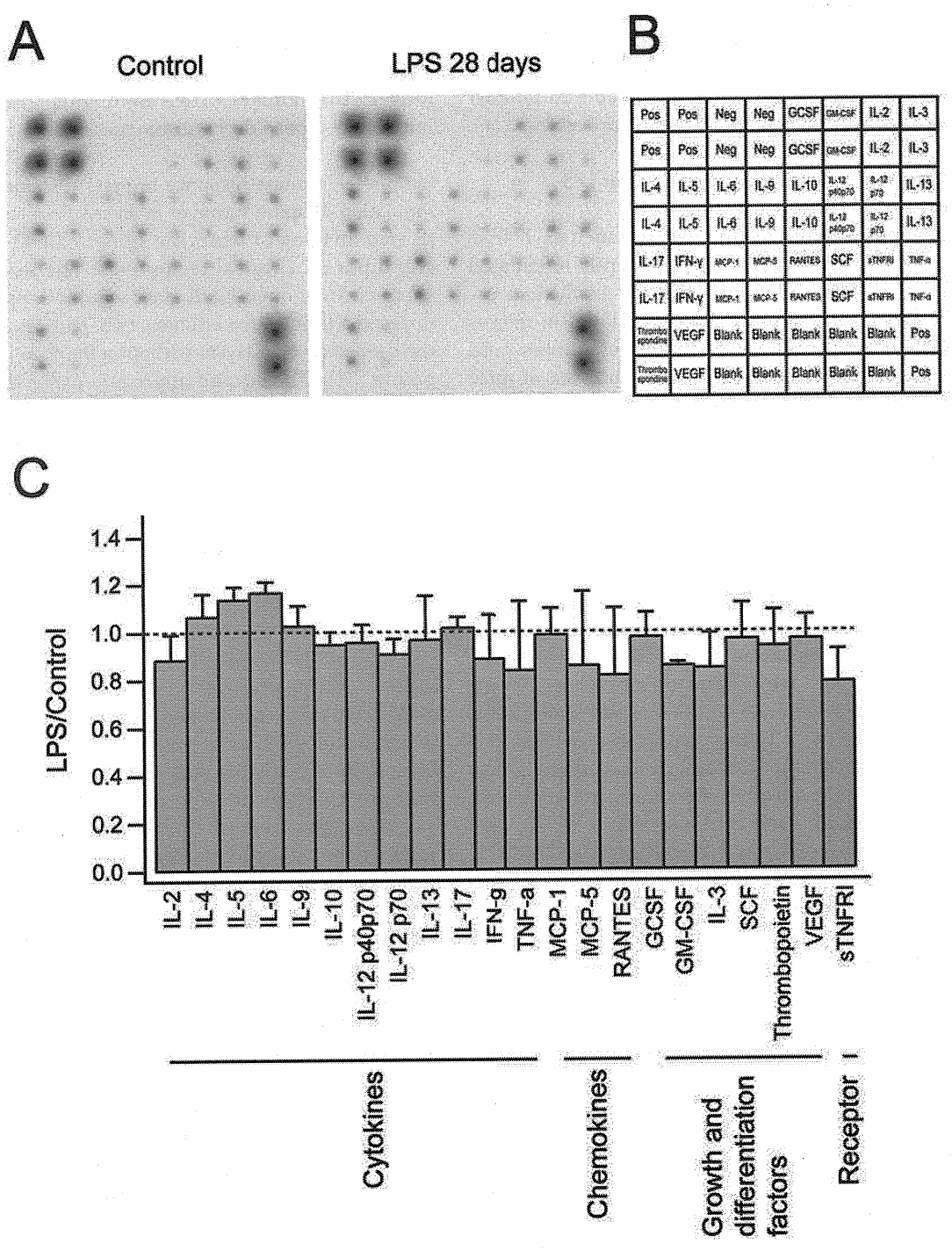

Figure 8 Brain cytokine expression after LPS treatment. (A) Images of cytokine array membranes incubated with brain homogenates from control mice (N = 3) and mice treated with LPS 28 days before preparation of brain homogenates (N = 3). (B) The arrangement of tested cytokines on the membrane. (C) The density of each spot was measured and the ratios between control and LPS-treated groups were calculated. There was no substantial increase or decrease in expression of the cytokines we tested.

[40,41]. Therefore changes in synaptic connections should be associated with functional changes in the neural network. Then, what are the functional outcomes of spine dynamics after LPS treatment? Interestingly, Sparkman *et al.* reported that LPS administration affected the performance of mice in the Morris water maze more profoundly on later test days [39]. The difference in distance swam became significant only after three days had elapsed following LPS injection. This time course may reflect accumulation of network remodeling in the hippocampus over the period of several days, which may be paralleled by the enhanced spine turnover we observed in the neocortex. A possible link between cognitive impairment observed in LPS-treated rodents and alterations in the neural network is reinforced by a previous study showing LPS-dependent modification of synaptic plasticity, such as LTP [9]. For example, Shaw *et al.* reported impairment of both the dentate gyrus LTP *in vivo* and performance of a water maze task in rats that received a single dose of LPS (0.25 mg/kg) intraperitoneally [42]. Cytokines up-regulated by LPS administration, such as TNFα and IL-1β, are also known to function as modulators of synaptic plasticity [43-45]. It is possible that elevation of cytokines initiated by peripheral LPS treatment modulates LTP/long-term depression (LTD)-like mechanisms *in vivo* and subsequently triggers structural remodeling of the neural network, including addition and elimination of spines.

Persistent microglial activation triggered by peripheral immune responses may be involved in enhanced spine dynamics

Neuronal networks in the mammalian forebrain are intrinsically dynamic [20,46] and are regulated by interactions with glia [19,47-49]. Microglial cells constitute the major cell type which responds to peripheral inflammation in the CNS [37]. Therefore we suspected that microglial cells directly modulated spine dynamics in response to intraperitoneal administration of LPS. As we already discussed, *in vivo* imaging through an open-skull glass window results in relatively high turnover rate of spines, together with transient activation of microglia. In contrast, with the thinned-skull window technique, much less spine dynamics and microglia activation were observed [32]. In pathological states, microglial processes show enhanced motility [17,18] and preferentially associate with synapses and may facilitate their deconstruction [19]. How microglia regulate neural networks *in vivo* is still poorly understood. Microglia may induce synapse remodeling via direct mechanical contact of their processes with synapses, or they may release soluble factors which destabilize nearby synapses. In order to evaluate these possibilities, we performed morphological and biochemical analyses of microglia in the neocortex after LPS administration.

In order to address the structural interactions between microglia and spines, we first analyzed the morphological transition of microglia with enhanced Iba1 expression after LPS administration. Iba1 is a small EF hand calcium binding protein involved in Rac and calcium signaling pathways [15]. Therefore, morphological changes of microglia could be related to the reorganization of the actin network through the Rac pathway. We observed both enhanced Iba1 expression and shrinkage of microglial processes two days after LPS treatment. This observation confirms that a single peripheral injection of LPS is sufficient to trigger activation of microglia. Iba1 expression was up-regulated between seven and 28 days after LPS administration and the number of microglia was also increased during the same period. These observations are consistent with the idea that microglia activation is not only maintained, but gradually enhanced over a time period of several weeks after LPS treatment. Our *in vivo* imaging of *Iba1-GFP* mice revealed that microglial processes had comparable motility before and after LPS treatment. Because the density of microglia increased late after LPS treatment, the frequency of individual synapses to receive contact of activated microglia may also be enhanced. This effect possibly underlies the progressive elimination of spines after LPS treatment. In the current studies, we restricted our analysis of microglial changes up to one month and we did not investigate the direct association between dendritic spines and microglial processes. However, the dynamic nature of microglial processes and their interaction with synapses were reported recently (17-19). Our present observation of the alterations in spine remodeling suggests an association with the change in microglia. Further studies are necessary to elucidate whether microglial contact is involved in the spine elimination.

Cytokines that are secreted from glial cells in the brain can affect both synaptic functions and spine morphology [43,44,50]. In animal models of neurodegenerative disorders and aging, there are reports of proliferating activated microglia and the increased levels of proinflammatory and anti-inflammatory cytokines together with impairments of spine density and morphology [51]. Systemic administration of LPS also increases several types of cytokines in the peripheral blood, mainly TNF-α, IL-1β, and IL-6 [7]. In order to detect soluble factors up-regulated in the brain during the persistent enhancement of spine turnover, we measured the levels of cytokines and chemokines in brain extracts prepared 28 days after LPS treatment. However, we were unable to detect increased expression of multiple cytokines. These results suggest that either signals